This document is the Accepted Manuscript version of a Published Work that appeared in final form in *Crystal Growth and Design*, copyright © American Chemical Society after peer review and technical editing by the publisher.

To access the final edited and published work see: https://doi.org/10.1021/acs.cgd.7b00525

Growth of twin-free and low-doped topological insulators on $BaF_2(111)$

Frédéric Bonell[1]*, Marc G. Cuxart[1,2], Kenan Song[1,2], Roberto Robles[1], Pablo Ordejón[1], Stephan Roche[1,3], Aitor Mugarza[1,3] and Sergio O. Valenzuela[1,3]*

[1] Catalan Institute of Nanoscience and Nanotechnology (ICN2), CSIC and The Barcelona Institute of Science and Technology, Campus UAB, Barcelona 08193, Spain

[2] Universitat Autònoma de Barcelona (UAB), Bellaterra, 08193, Spain

[3] Institució Catalana de Recerca i Estudis Avançats (ICREA), Barcelona 08070, Spain

We demonstrate the growth of twin-free Bi_2Te_3 and Sb_2Te_3 topological insulators by molecular beam epitaxy, and a sizable reduction of the twin density in Bi_2Se_3, on lattice-matched $BaF_2(111)$ substrates. Using x-ray diffraction, electron diffraction and atomic force microscopy, we systematically investigate the parameters influencing the formation of twin domains and the morphology of the films, and show that Se- and Te-based alloys differ by their growth mechanism. Optimum growth parameters are shown to result in intrinsically low-doped films, as probed by angle-resolved photoelectron spectroscopy. In contrast to previous approaches, in which twin-free Bi_2Se_3 films are achieved by increasing the substrate roughness, the quality of our Bi_2Te_3 is superior on the flattest BaF_2 substrates. This finding indicates that, during nucleation, the films not only interact with the topmost atomic substrate layer but also with buried layers that provide the necessary stacking information to promote a single twin, an observation that is supported by *ab-initio* calculations.

Bismuth and antimony chalcogenides, Bi_2Te_3, Sb_2Te_3 and Bi_2Se_3, are prototypical topological insulators (TIs), a new class of bulk insulators with conductive surface states.[1-3] Their surface hosts Dirac fermions protected by time-reversal symmetry and characterized by spin-momentum locking, a property that prevents backscattering and that is highly attractive for spintronics and fault-tolerant quantum computation.[3,4] However, bismuth and antimony chalcogenides are narrow gap semiconductors that are very sensitive to doping, and the surface currents are typically overwhelmed by bulk currents. In order to favour surface transport, it is necessary to suppress the bulk conductivity, which requires the growth of low-defect thin films, a task that has proven to be very challenging.[5-9] Due to doping by impurities or crystalline defects, the Fermi level of Bi_2Se_3 and Bi_2Te_3 is typically shifted to the conduction band.[5,8,10-14] Although counter-doping or electrostatic gating may be used to tune the Fermi energy, structural defects impact negatively the transport properties by coupling surface and bulk channels, by reducing the carrier mobility or by suppressing the surface states in the case of strain localized at grain boundaries.[15] Some common imperfections are Se/Te vacancies, dislocations, mosaïcity, 30° rotational domains and twin domains.[5,7,15-18] In particular, mirror-symmetric twin domains are of special importance owing to the extended planar nature of their boundaries (see **Figure 1a**). They are known to introduce electron scattering, strain and doping in various semiconductors such as GaAs[19] or HgCdTe.[20] In TIs, it has been demonstrated that twin boundaries hold a spontaneous polarization responsible for self-doping of the surface states, which may reach several hundreds of meV.[21]

TIs are usually grown on conventional substrates such as $Al_2O_3(0001)$[7,10,13,22] and $Si(111)$,[8,13,14,23-26] despite lattice misfits close to 15%. On such substrates, the growth generally proceeds by the formation of a polycrystalline or amorphous seed layer,[7,18,25] followed by the growth of a (0001)-textured film in which 30° rotational domains and twins

3

are inevitably present. Lattice-matched InP(111) (0.2% misfit) was shown to ensure a much better crystallinity of Bi_2Se_3, characterized by reduced mosaïcity twist and the suppression of 30° domains.[7,18] On flat InP(111) substrates, a reduction of twinning was also observed, with the dominant twin occupying 66% of the total volume.[6] Further reduction down to full suppression of the minority twin was achieved by the use of rough substrates, at the expense of additional antiphase domains and, possibly, increased roughness of the films. Notably, twin suppression correlated with a reduction of the carrier density by almost one order of magnitude, demonstrating the relevance of structural improvement to achieve superior transport properties.[6] Suppression of twinning was also realized in Bi_2Te_3 grown at very low rate on Te-passivated Si(111), showing that improvement of the crystallinity can be achieved by controlling the growth kinetics.[8] In this case, single crystal epitaxy was likely promoted by the 7:8 incommensurate matching of the Si and Bi_2Te_3 lattices (1% misfit). Nonetheless, no reduction in the carrier concentration could be observed: the films remained highly n-doped, which suggests that the incommensurate epitaxy was not able to suppress other kinds of structural imperfections. Lower doping was obtained by growing Bi_2Te_3 on lattice-matched $BaF_2(111)$ (0.1% misfit),[9,11,27,28] but complete suppression of twinning has never been reported.

In the present study, we demonstrate the growth of twin-free Te-based TIs (Bi_2Te_3 and Sb_2Te_3) on flat $BaF_2(111)$ substrates. Contrary to the growth on Te-passivated Si(111), full suppression of twinning is accompanied with very low doping levels, as demonstrated with angle-resolved photoelectron spectroscopy (ARPES). We achieve twin-free films by investigating their growth mechanism as a function of the temperature, in combination with systematic characterization using atomic force microscopy (AFM), electron diffraction (RHEED) and X-ray diffraction (XRD), to quantify the twin density and the desorption

process. Sizable twin suppression is also achieved in Bi_2Se_3, with noticeable improvement compared to the growth on flat InP(111) substrates.

Topological insulator thin films were grown by coevaporation of elemental Bi, Sb, Se and Te (6N purity) in a molecular beam epitaxy chamber with a base pressure of 2×10^{-10} mbar and equipped with a 15 keV RHEED system. Bi, Sb and Te were thermally cracked. Consequently, the optimal Te/Bi and Te/Sb flux ratios were found to be around 2, slightly larger than the stoichiometric ratio of 1.5 for Bi_2Te_3 and Sb_2Te_3, and much lower than flux ratios of 10-20 generally used without cracker cells. Se was evaporated from a low temperature effusion cell at 210°C and a Se/Bi flux ratio around 10 was used. The effusion cell/cracker temperatures were 570/1100°C for Bi in Bi_2Te_3, 510/1100°C for Bi in Bi_2Se_3, 280/600°C for Te and 370/850°C for Sb. The fluxes were measured by a previously calibrated quartz crystal microbalance. Prior to the deposition, epi-ready $BaF_2(111)$ substrates (*Crystal GmbH*) were outgassed in ultra-high vacuum (UHV) at 800°C during 1 hour. All TI films were grown in a single step and were nominally 9 QL-thick. The growth rates measured by recording QL-periodic RHEED intensity oscillations were 0.12 QL/min for Bi_2Se_3 and 0.28 QL/min for Bi_2Te_3 and Sb_2Te_3. AFM and X-ray diffraction experiments were performed on the bare films exposed to air. AFM images were recorded a few hours after the growth in order to ensure minimal contamination. X-ray diffraction and reflectivity measurements were performed on a PANalytical X'Pert Pro diffractometer operating with Cu K_α radiation. For ARPES measurements, the films were capped with a 15 nm-thick Te layer deposited below 100°C, then exposed to air and transferred in few minutes from the MBE to the ARPES chamber. The Te cap layer was desorbed by heating the sample during 10 min at 190°C in UHV ($< 10^{-9}$ mbar). This procedure has been shown to introduce virtually no doping of the surface states.[28] X-ray photoelectron spectroscopy (XPS) was used to check the complete removal of the capping, to confirm the absence of oxidation, and to control the film

composition (Bi/Te ratio found equal to 2/3 within the experimental uncertainty). ARPES was performed with He I radiation (21.22 eV) in UHV ($< 5 \times 10^{-10}$ mbar).

To quantify the density of twins we used *in-situ* RHEED measurements and *ex-situ* XRD characterization. **Figure 1b** and **1c** summarize the results for a Sb_2Te_3 film grown at 400°C and two series of films grown at various temperatures T_G in the range 200°C-280°C for Bi_2Se_3 and 300°C-500°C for Bi_2Te_3. Despite being a technique that is intrinsically sensitive to the surface, in **Figure 1b** we demonstrate that RHEED provides qualitative real-time information on the twin density because of the large penetration depth of high energy electrons along their propagation direction. The position of diffraction rods is broadly characterized by a 6-fold symmetry, which reflects the hexagonal symmetry of the topmost atomic layer, independently of the stacking order. However, because of their finite penetration depth, electrons can be transmitted through islands of few tens of nanometers and are able to trace twins that differ by their ABCAB or ACBAC stacking (**Figure 1a**). As a result, the intensity along the rods is modulated, with maxima corresponding to 3D Bragg conditions and reflecting the trigonal symmetry of the crystal (details in the **Supporting Information**). The modulation is visible in all our RHEED measurements and is highlighted with arrows in **Figure 1b**. In all cases, RHEED shows the absence of 30° rotational domains, which would result in mixed $[1\bar{1}00]$ and $[11\bar{2}0]$ patterns. In the case of Bi_2Te_3 and Sb_2Te_3, the $[11\bar{2}0]$ diffraction patterns are invariant under a 120° rotation, whereas a 60° rotation results in mirror-symmetric images. Therefore one twin is dominant. Bi_2Se_3 patterns present intensity maxima corresponding to a combination of the two variants, showing that the two twins are present in these films.

Remarkably, the RHEED patterns of both Bi_2Te_3 and Bi_2Se_3 ultrathin films of just 0.5 QL display the characteristic diagonal modulation of a twin-free crystal (**Figure 1b**), which

shows that the $BaF_2(111)$ surface forces the nucleation of islands with a definite stacking. This also demonstrates excellent epitaxy since the very first stages of the growth, and a $BaF_2(111)$/TI interface of high quality, which is in clear contrast with the 1-2 QL-thick amorphous or partly disordered seed layers observed on $Al_2O_3(0001)$, $Si(111)$ and even $InP(111)$.[6,7,18] Bi_2Te_3 keeps this structure during subsequent deposition, whereas twins gradually appear in Bi_2Se_3 indicating a change of the stacking in the growth direction (lamellar twins). The difference between Bi_2Te_3 and Bi_2Se_3 may be a consequence of the different T_G, which results in different diffusion lengths of surface species and/or by a weaker inter-layer bonding in Bi_2Se_3. However, increasing the growth temperature of Bi_2Se_3 does not result in better crystallinity, as will be discussed below.

In order to quantify the degree of twinning, we measured pole scans of the $\{10\bar{1}5\}$ reflections by XRD. Twin-free films should yield 3-fold symmetric scans, while films containing twins in equal proportion are expected to show a perfect 6-fold symmetry, with equal intensity peak triplets at 60, 180 and 300° and at 0, 120 and 240°. The diffraction intensity for specific T_G is shown in **Figure 1c**. For all T_G, we observe that the intensity at 60, 180 and 300° is always stronger than at 0, 120 and 240°, indicating that one twin is dominant. The most intense reflections occur systematically at 60° of the $\{002\}$ BaF_2 reflections, revealing that the ABC stacking of the $BaF_2(111)$ substrate tends to be conserved in the grown TI and confirming that the dominant twin is determined by interaction with the substrate. In **Figure 2a,** we show the proportion of the minority twin, which we obtain by dividing the integrated intensity of the corresponding peak triplet in **Figure 1c** to the total intensity. In the case of Bi_2Te_3, an increase in T_G above 300°C leads to a reduction in the twin density, down to a complete suppression at 375°C. As observed in **Figure 2b**, the suppression of twins correlates with a sudden decrease of the peaks linewidth (from 3.0° at 300°C down to 0.8° at 400°C), which denotes a sharp reduction of the mosaïcity twist. Similarly to Bi_2Te_3, Sb_2Te_3 grown at 400°C

shows narrow XRD peaks (1.4°) and a very small proportion of the minority twin (3%). In contrast, the Bi_2Se_3 films are in general more defective, as inferred from the linewidth of XRD and RHEED reflections, which are similar to those observed with Bi_2Te_3 grown at low temperature (2.0° at 220-235°C). The twin density in Bi_2Se_3 is characterized by a non-monotonous temperature dependence (**Figure 2a**). The minimum density is observed at 220°C, for which the majority twin represents 76% of the volume of the film. Even though full twin suppression is not achieved, this represents a sizable improvement in comparison to the proportion of 66% achieved on flat InP(111).[6]

In order to understand the differences between the growth of Bi_2Se_3 and the Te-based alloys, and to gain insight into the mechanism of twin formation, we performed systematic AFM measurements of the deposited films as a function of T_G in substrates with different roughness (epi-ready and cleaved). **Figure 3** shows the typical films morphologies as a function of T_G. As has been previously reported, we observe spiral-like growth and steps with 1 QL height.[16,30] Bi_2Te_3 presents triangular islands, denoting an anisotropic growth rate in $[1\bar{1}00]$ and $[11\bar{2}0]$ directions. Below 350°C, the triangular islands can be oriented in two opposite directions, depending on the twin orientation.[6,7,31] From the AFM images, it is apparent that twinning is partially suppressed in Bi_2Te_3 and the size of the islands increases when increasing T_G from 300°C to 350°C. For $T_G > 400$°C, islands are merged, which means that the diffusion length of the adatoms is of the order of the terrace width. Therefore, the sharp decrease of the mosaïcity twist and the full suppression of twinning occur at the onset of islands coalescence. Further increase of the growth temperature results in larger terraces. Bi_2Se_3 presents more hexagonal islands, with a density that reaches a minimum at 220°C and increases significantly at higher T_G. The spirals density for both Bi_2Se_3 and Bi_2Te_3 was estimated from AFM images like those shown in **Figure 3**, and is reported in **Figure 2c**. The

similar trends observed in **Figure 2a** and **2c** demonstrate a large correlation between the spiralling islands density and twinning.

These observations show that the growth mechanism for Bi_2Te_3 and Bi_2Se_3 at elevated temperatures is different. Bi_2Te_3 grows initially by diffusion-nucleation; higher temperatures promote the diffusion of surface species and lead to extended islands. Following initial nucleation, the enhanced diffusion promotes spiral-like growth, without noticeable nucleation, as we do not observe RHEED oscillations. Incoming species stick to the terrace edges, ensuring the conservation of the stacking order and the absence of twinning. For Bi_2Se_3, the increase of spiral density for $T_G > 220°C$ is unconventional. It suggests a reaction-limited nucleation mechanism due to the instability of Se upon desorption. Such a mechanism has been reported in the growth of GaAs.[32] In this case, the instability of Ga-As precursors upon As desorption leads to an excess of Ga adatoms at the surface, which act as new nucleation centers. As a result, increasing desorption of As at higher T_G leads to a higher nucleation density. It is likely that a similar mechanism occurs with Bi_2Se_3 since Se has a much higher vapour pressure than Bi. This leads to the desorption of Se and an excess of Bi at moderate temperatures, without affecting the growth rate which is limited by the Bi supply (**Supporting Information**). The instability of surface species and the continuous nucleation have the additional consequence of randomizing the atomic configuration, which prevents us from reaching pure spiral-like growth and results in a finite probability of twinning. Nonetheless, the epitaxy remains of good quality since 30° domains are completely absent even at high temperature.

Figure 4 compares the AFM images and pole scans of two films grown at 350°C onto epi-ready and cleaved BaF_2, respectively. The very (111) surface plane of BaF_2 has hexagonal symmetry and should in principle lead to the formation of both twins with equal probability. To induce single-twin growth, 3D information from the substrate must be transferred to the

epilayer, either through the contribution of the sub-surface plane to the adsorption potential[8] or by interaction with the atomic steps present on the substrate.[6] The surface of epi-ready substrates systematically shows a high density of nm-deep pits stemming from the chemo-mechanical polishing process, which are readily observable in the topography of the films (**Figure 4a**). In contrast, the surface of cleaved $BaF_2(111)$ is atomically flat over tens of micrometres while no pits are found (**Figure 4b**). In spite of this, the surface condition of the substrate has a negligible influence on the islands density. Moreover, the growth on cleaved substrates results in further improvement of the film crystallinity, as inferred from the much sharper diffraction peaks and the full suppression of twinning at moderate growth temperature (**Figure 4e** and **4f**). This implies that instead of promoting single-twin growth, as reported for growth in InP(111) [6], the surface roughness tends to pin disoriented domains, while the atomically flat substrate extends the optimal T_G window to lower temperatures.

The direct interaction between BaF_2 and Bi_2Te_3 therefore promotes single twin growth. In order to further support this conclusion, we performed DFT calculations of $BaF_2(111)/Bi_2Te_3(1$ QL) slabs with the two possible stacking orders (details in the **Supporting Information**). The energy difference between the two configurations amounts to 5 meV/cell (2 mJ/m^2) in favour of the experimentally observed dominant twin. Whether such a small difference can eventually account for the complete twin suppression is not clear, but it definitely favours one stacking configuration. In addition, the calculations confirm the low chemical interaction between Bi_2Te_3 and $BaF_2(111)$, with a charge transfer of only 0.15 e$^-$/cell and a binding energy dominated by the Van der Waals interaction (+392 meV/cell).

Finally, ARPES intensity maps of twin-free Bi_2Te_3 grown under optimized conditions ($T_G = 380°C$) demonstrate very low doping levels, with the Fermi level lying 80 meV below the conduction band minimum at room temperature (**Figure 5a**). At 80 K, sizable downward band bending is observed, as commonly reported for ageing of TI surfaces,[29] but the Fermi

level remains in the bulk gap and intersects only the topological surface states (**Figure 5b**). In contrast, the Fermi level of Bi_2Te_3 grown at $T_G = 250°C$ lies in the conduction band, which demonstrates the large electron doping introduced by crystal defects such as mosaïcity, twinning and roughness (**Figure 5c**).

CONCLUSIONS

In summary, we have shown that lattice-matched $BaF_2(111)$ substrates enable the growth of high quality TIs by molecular beam epitaxy, with an excellent $BaF_2(111)/Bi_2Te_3$ interface quality. The complete suppression of twins is achieved in Bi_2Te_3 and Sb_2Te_3 by a combination of the initial interaction with the substrate and the spiral-like growth mode favoured by high working temperatures. As a result, Bi_2Te_3 films are shown to be exceptionally low-doped, with their Fermi level well within the bulk band gap. Such a low doping contrasts with measurements of twin-free $Si(111)/Bi_2Te_3$, for which the Fermi level lies in the conduction band.[8] This shows that the growth on lattice-matched $BaF_2(111)$ results in a general structural improvement, preventing the formation of defects that cannot be suppressed by the incommensurate epitaxy on $Si(111)$. Bi_2Se_3 also shows superior structural quality compared to films grown on other substrates but, despite initial single-twin nucleation at the $BaF_2(111)$ surface, the formation of twin defects during subsequent Bi_2Se_3 homoepitaxy could not be completely avoided. A growth instability due to Se desorption at high temperature is responsible for the nucleation of new islands and the associated formation of twin domains. Since growth kinetics and desorption play a central role, further improvement might be simply achieved by deposition at lower rates and higher Se fluxes.

SUPPORTING INFORMATION

Desorption and temperature dependence of the growth rate, simulated RHEED patterns, *ab initio* calculations of interface energies.

AUTHOR INFORMATION

Corresponding author

*E-mail: frederic.bonell@icn2.cat; SOV@icrea.cat

ACKNOWLEDGEMENTS

REFERENCES

[1] H. Zhang, C.-X. Liu, X.-L. Qi, X. Dai, Z. Fang, S.-C. Zhang, Nature Phys. **2009**, 5, 438.

[2] M. Z. Hasan, C. L. Kane, Rev. Mod. Phys. **2010**, 82, 3045.

[3] *Topological Insulators, Fundamentals and Perspectives.* F. Ortmann, S. Roche, S. O. Valenzuela Eds. (Wiley, 2015).

[4] L. He, X. Kou, K. L. Wang, Phys. Status Solidi RRL **2013**, 7, 50.

[5] J. Dai, D. West, X. Wang, Y. Wang, D. Kwok, S.-W. Cheong, S. B. Zhang, W. Wu, Phys. Rev. Lett. **2016**, 117, 106401.

[6] N. V. Tarakina, S. Schreyeck, M. Luysberg, S. Grauer, C. Schumacher, G. Karczewski, K. Brunner, C. Gould, H. Buhmann, R. E. Dunin-Borkowski, L. W. Molenkamp, Adv. Mater. Interfaces **2014**, 1, 1400134.

[7] A. Richardella, A. Kandala, J. S. Lee, N. Samarth, APL Mater. **2015**, 3, 083303.

[8] J. Kampmeier, S. Borisova, L. Plucinski, M. Luysberg, G. Mussler, D. Grützmacher, Cryst. Growth Des. **2015**, 15, 390.

[9] C. I. Fornari, P. H. O. Rappl, S. L. Morelhão, Eduardo Abramof, J. Appl. Phys. **2016**, 119, 165303.

[10] C.-Z. Chang, K. He, L.-L. Wang, X.-C. Ma, M.-H. Liu, Z.-C. Zhang, X. Chen, Y.-Y. Wang, Q.-K. Xue, SPIN **2011**, 1, 21.

[11] O. Caha, A. Dubroka, J. Humlíček, V. Holý, H. Steiner, M. Ul-Hassan, J. Sánchez-Barriga, O. Rader, T. N. Stanislavchuk, A. A. Sirenko, G. Bauer, G. Springholz, Cryst. Growth Des. **2013**, 13, 3365.

[12] S. E. Harrison, S. Li, Y. Huo, B. Zhou, Y. L. Chen, J. S. Harris, Appl. Phys. Lett. **2013**, 102, 171906.

[13] J. Krumrain, G. Mussler, S. Borisova, T. Stoica, L. Plucinski, C. M. Schneider, D. Grützmacher, J. Cryst. Growth **2011**, 324, 115.

[14] Y.-Y. Li, G. Wang, X.-G. Zhu, M.-H. Liu, C. Ye, X. Chen, Y.-Y. Wang, K. He, L.-L. Wang, X.-C. Ma, H.-J. Zhang, X. Dai, Z. Fang, X.-C. Xie, Y. Liu, X.-L. Qi, J.-F. Jia, S.-C. Zhang, Q.-K. Xue, Adv. Mater. **2010**, 22, 4002.

[15] Y. Liu, Y. Y. Li, S. Rajput, D. Gilks, L. Lari, P. L. Galindo, M. Weinert, V. K. Lazarov, L. Li, Nature Phys. **2014**, 10, 294.

[16] H. Steiner, V. Volobuev, O. Caha, G. Bauer, G. Springholz, V. Holý, J. Appl. Cryst. **2014**, 47, 1889.

[17] G. Zhang, H. Qin, J. Chen, X. He, L. Lu, Y. Li, K. Wu, Adv. Funct. Mater. **2011**, 21, 2351.

[18] N. V. Tarakina, S. Schreyeck, T. Borzenko, C. Schumacher, G. Karczewski, K. Brunner, C. Gould, H. Buhmann, L. W. Molenkamp, Cryst. Growth Des. **2012**, 12, 1913.

[19] K. Shimamura, Z. Yuan, F. Shimojo, A. Nakano, Appl. Phys. Lett. **2013**, 103, 022105.

[20] J.P. Faurie, R. Sporken, S. Sivananthan, M.D. Lange, J. Cryst. Growth **1991**, 111, 698.

[21] H. Aramberri, J. I. Cerdá, M. C. Muñoz, Nano Lett. **2015**, 15, 3840.

[22] J. J. Lee, F. T. Schmitt, R. G. Moore, I. M. Vishik, Y. Ma, Z. X. Shen, Appl. Phys. Lett. **2012**, 101, 013118.

[23] X. Chen , X.-C. Ma, K. He, J.-F. Jia, Q.-K. Xue, Adv. Mater. **2011**, 23, 1162.

[24] S. Borisova, J. Kampmeier, M. Luysberg, G. Mussler, D. Grützmacher, Appl. Phys. Lett. **2013**, 103, 081902.

[25] N. Bansal, Y. S. Kim, E. Edrey, M. Brahlek, Y. Horibe, K. Iida, M. Tanimura, G.-H. Li, T. Feng, H.-D. Lee, T. Gustafsson, E. Andrei, S. Oh, Thin Solid Films **2011**, 520, 224.

[26] G. Wang, X.-G. Zhu, Y.-Y. Sun, Y.-Y. Li, T. Zhang, J. Wen, X. Chen, K. He, L.-L. Wang, X.-C. Ma, J.-F. Jia, S. B. Zhang, Q.-K. Xue, Adv. Mater. **2011**, 23, 2929.

[27] K. Hoefer, C. Becker, D. Rata, J. Swanson, P. Thalmeier, L. H. Tjeng, PNAS **2014**, 111, 14979.

[28] K. Hoefer, C. Becker, S. Wirth, L. H. Tjeng, AIP Advances **2015**, 5, 097139.

[29] K. Park, C. De Beule, B. Partoens, New Journal of Physics **2013**, 15, 113031.

[30] Y. Liu, M. Weinert, L. Li, Phys. Rev. Lett. **2012**, 108, 115501.

[31] H. D. Li, Z. Y. Wang, X. Kan, X. Guo, H. T. He, Z. Wang, J. N. Wang, T. L. Wong, N. Wang, M. H. Xie, New Journal of Physics **2010**, 12, 103038.

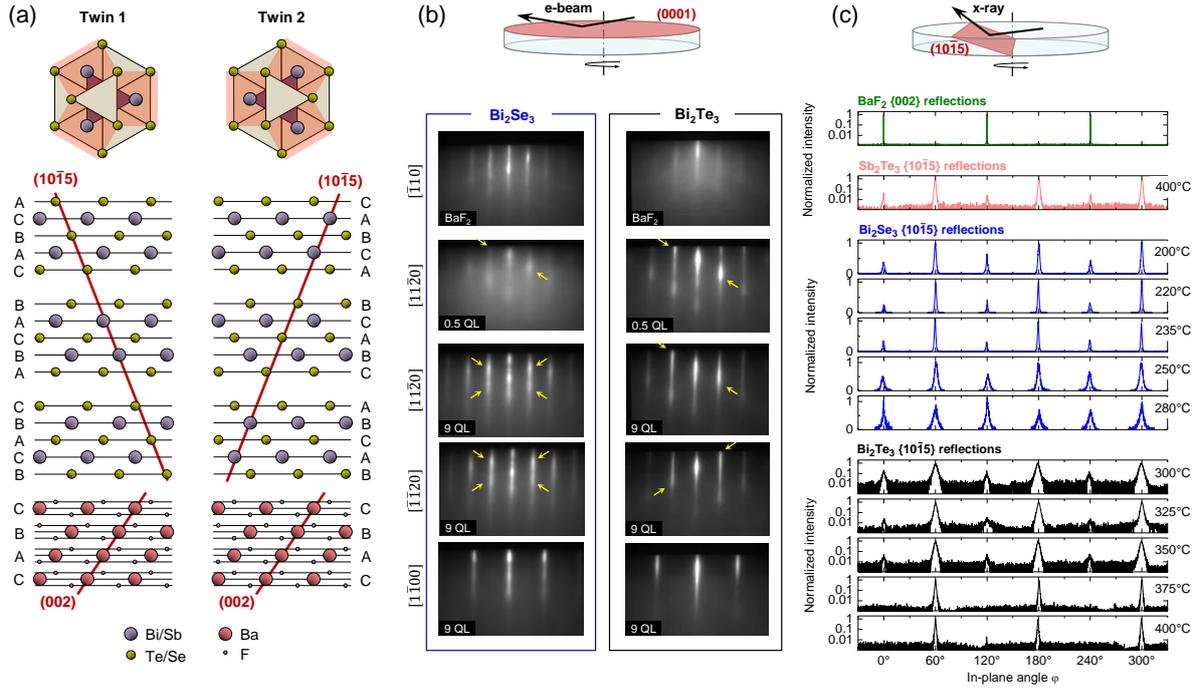**[32]** P. Kratzer, M. Scheffler, Phys. Rev. Lett. **2002**, 88, 036102.

Figure 1. (a) Atomic arrangement of the two twins occurring in (0001) TI ∥ (111) BaF$_2$ epitaxy (twin 1: $[10\bar{1}0]$ ∥ $[11\bar{2}]$; twin 2: $[\bar{1}010]$ ∥ $[11\bar{2}]$). The twins differ by their ABCAB or ACBAC stacking, as apparent in both the TI $(1\bar{2}10)$ side view and (0001) top view. $\{10\bar{1}5\}$ planes are highlighted in red; their 3-fold symmetry is visible in the top view. **(b)** RHEED patterns measured during the growth of Bi$_2$Se$_3$ at 235°C and Bi$_2$Te$_3$ at 400°C on BaF$_2$(111). The intensity modulation highlighted by arrows reveals the presence/absence of twin defects. 3-fold symmetric diffraction patterns of Bi$_2$Te$_3$ with a diagonal intensity modulation are characteristic of twin-free films, whereas 6-fold symmetric diffraction patterns of Bi$_2$Se$_3$ are indicative of a film composed of both twins. **(c)** X-ray diffraction pole scans of $\{002\}$ BaF$_2$ planes and $\{10\bar{1}5\}$ TIs planes, for different growth temperatures. Each twin results in one peak triplet (twin 1: 60°, 180° and 300°; twin 2: 0°, 120° and 240°). Intensity scales are logarithmic for BaF$_2$, Bi$_2$Te$_3$, and Sb$_2$Te$_3$ (quasi-single-twin), and linear for Bi$_2$Se$_3$ (larger twin density).
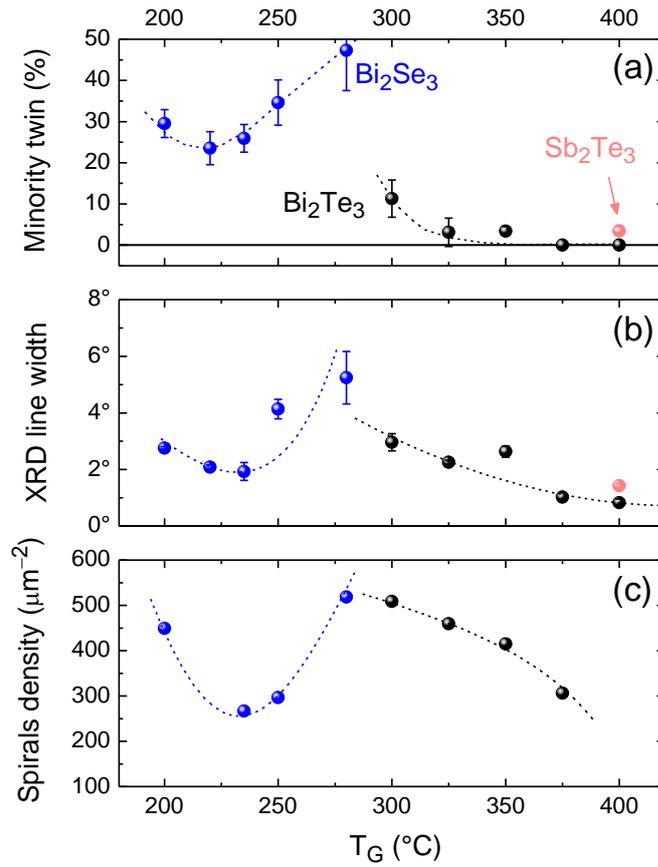
Figure 2. Dependence of TIs thin films properties on the growth temperature. Optimal growth is found around 220°C for Bi_2Se_3 and 375°C-400°C for Bi_2Te_3. **(a)** Proportion of minority twin domains determined from the X-ray diffraction pole scans shown in Figure 1c. **(b)** Line width of the diffraction peaks in pole scans. **(c)** Density of spiralling islands estimated from AFM images.
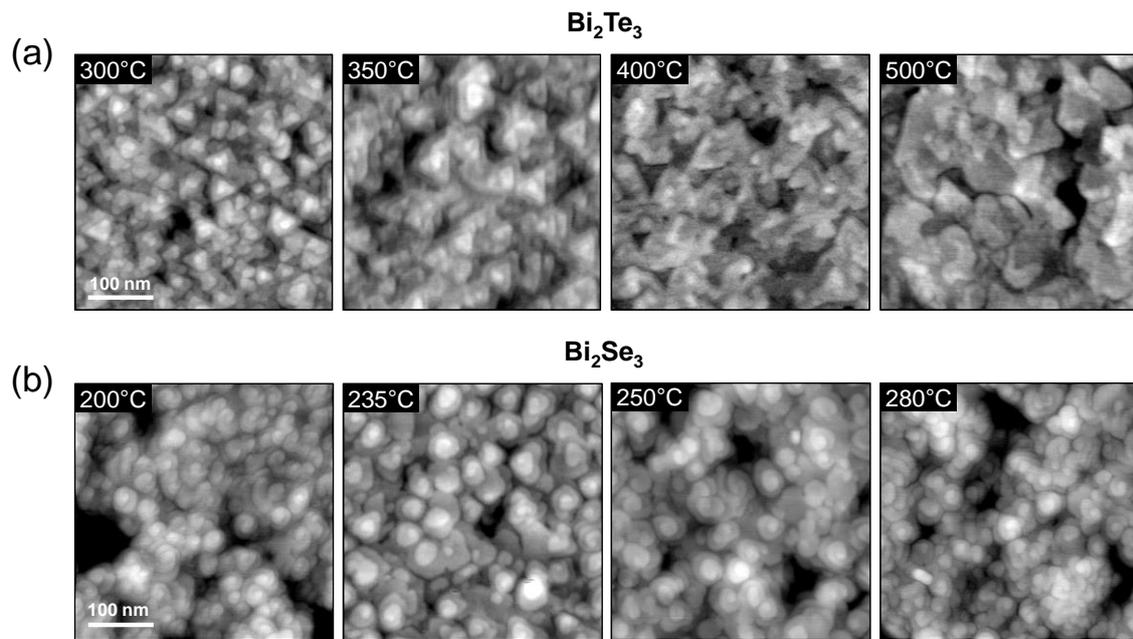
Figure 3. AFM images of nominally 9 QL-thick (a) Bi_2Te_3 and (b) Bi_2Se_3 grown at the indicated temperatures. All images are 400x400 nm^2. Triangular islands with opposite orientations are twin domains.
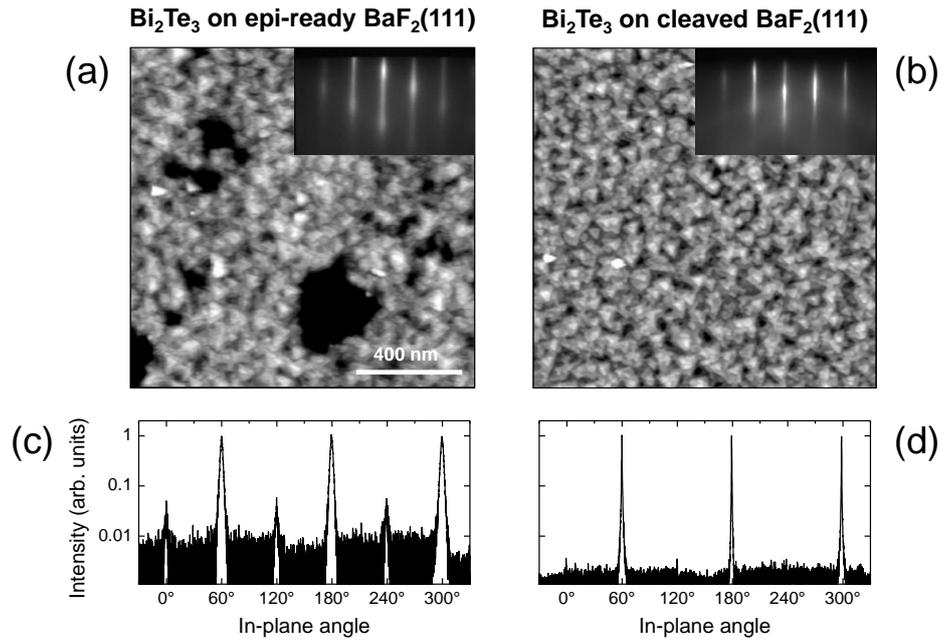
Figure 4. (a,b) AFM images and $[11\bar{2}0]$ RHEED patterns of 9 QL-thick Bi_2Te_3 thin films deposited at 350°C (a) on chemo-mechanically polished (epi-ready) $BaF_2(111)$ and (b) on cleaved $BaF_2(111)$. Epi-ready substrates display nm-deep pits due to the polishing process. **(c,d)** $\{10\bar{1}5\}$ X-ray diffraction pole scans associated to images (a,b). On epi-ready substrates, two twins are present. Growth on cleaved substrates results in sharper diffraction lines and in complete suppression of twin defects.
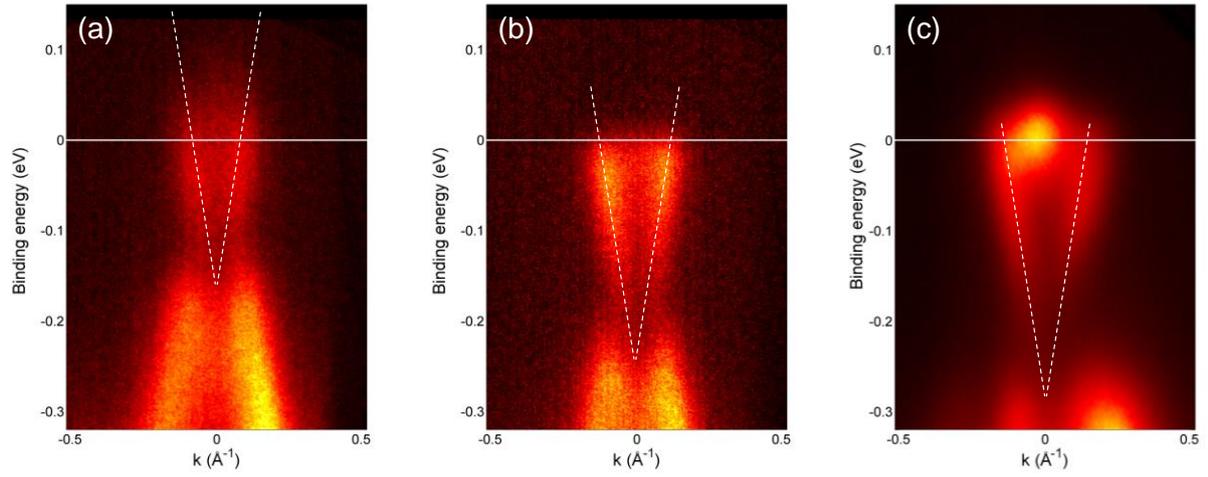
Figure 5. ARPES intensity maps of Bi_2Te_3 thin film in the Γ-K direction. (a) Low-doped, twin-free film grown at $T_G = 380°C$, measured at 300 K. (b) Same film measured at 80 K. (c) N-doped defective film deposited at $T_G = 250°C$; measured at 80 K.

Supporting Information

Growth of twin-free and low-doped topological insulators on BaF$_2$(111)

Frédéric Bonell[1], Marc G. Cuxart[1,2], Kenan Song[1,2], Roberto Robles[1], Pablo Ordejón[1],

Stephan Roche[1,3], Aitor Mugarza[1,3] and Sergio O. Valenzuela[1,3]

[1] Catalan Institute of Nanoscience and Nanotechnology (ICN2), CSIC and The Barcelona Institute of Science and Technology, Campus UAB, Barcelona 08193, Spain

[2] Universitat Autònoma de Barcelona (UAB), Bellaterra, 08193, Spain

[3] Institució Catalana de Recerca i Estudis Avançats (ICREA), Barcelona 08070, Spain

S1. Growth rate and desorption

We found that pure Se and Te hardly stick on BaF$_2$(111) at temperatures higher than 180°C and 370°C, respectively. However, optimal epitaxial growth requires keeping the substrate at temperatures slightly higher than those ones. To check whether this affects the growth rate, we measured the thickness of the deposited films by X-ray reflectivity, all the films having been grown with the same deposition time. We further normalized the growth rate to the rate inferred from RHEED intensity oscillations recorded at low temperature, where persistent diffusion-nucleation growth occurs. The normalized growth rates are reported in **Figure S1**. In the case of Bi$_2$Te$_3$, the deposition rate is constant up to 400°C and decreases for higher growth temperatures. This means that the sticking coefficient drops, or that the desorbed flux starts to overcome the adsorbed flux. It is well known that the growth rate is primarily determined by the Bi supply. Therefore, our measurements indicate that sizable desorption or incomplete sticking of Bi occurs above 400°C. As a result, the temperature window for optimized growth, determined by the trade-off between incomplete sticking and twin suppression, is found between 350°C and 400°C. The deposition rate of Bi$_2$Se$_3$ is found to be temperature independent despite the growth instability occurring above 220°C. The constant growth rate reflects the fact that Bi fully sticks to the surface and is hardly desorbed in this temperature range. This is further evidence that the growth instability and the increased nucleation density are due to Se

desorption, as discussed in the main text. Since Se is supplied in excess, the growth rate is not limited by its incoming flux.
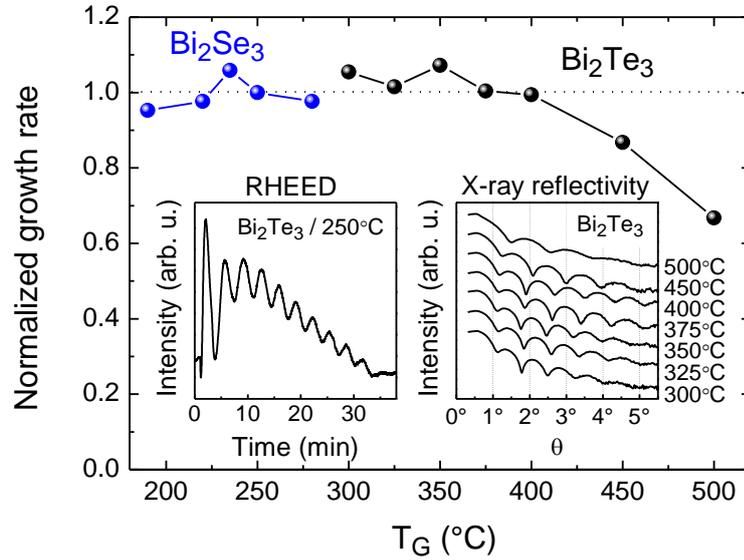

Figure S1. Growth rate normalized to the rate measured by RHEED intensity oscillations at low temperature (inset). The rates are derived from the deposition time and the final thickness of the films measured by X-ray reflectivity (inset).

S2. Calculated RHEED patterns

The diagonal intensity modulation in RHEED patterns of twin-free films is well reproduced by calculations using the kinematic diffraction theory. We estimated the intensity $I(\mathbf{r_S})$ at the positions $\mathbf{r_S}$ on the fluorescent screen from the following relations:

$$I(\mathbf{r}_S) \propto \left| \sum_{j,p} \kappa_p f_p \exp\left[-2\pi i \mathbf{q_{j,p}} \cdot \mathbf{r_{j,p}}\right] \right|^2,$$

$$\mathbf{q_{j,p}} = \mathbf{k_d}(j,p) - \mathbf{k_i}(j,p), \qquad \mathbf{k_i}(j,p) = k\frac{\mathbf{r_{j,p}} - \mathbf{r_E}}{\left|\mathbf{r_{j,p}} - \mathbf{r_E}\right|}, \qquad \mathbf{k_d}(j,p) = k\frac{\mathbf{r_S} - \mathbf{r_{j,p}}}{\left|\mathbf{r_S} - \mathbf{r_{j,p}}\right|},$$

where $\mathbf{k_i}$ and $\mathbf{k_d}$ are the incident and diffracted wavevectors, respectively. $\mathbf{q}$ is the scattering vector. The center of the screen and the position of the electron source $\mathbf{r_E}$ were both set at 20 cm from the crystal. $\mathbf{r_{j,p}}$ is the position of atom j in the atomic plane p and f_p its scattering factor (we assumed $f_{Bi}/f_{Te} = 1.2$). The summation was done over an area of 4×4 nm^2, which is the order of magnitude of the electron beam coherence length. The incidence angle of the electron beam was set to 2.5° and its energy to 10 keV ($k = 51.2$ Å). To account for the effect of 3D diffraction by transmission through islands, we assumed a finite penetration of the beam in the direction normal to the surface: $\kappa_p = \exp(-p/\lambda)$. When $\lambda \ll 1$, sub-surface planes do not contribute to diffraction so that no modulation is observed along the rods and the patterns are invariant through 60° rotation. We used $\lambda = 0.7$ for the calculated patterns shown in **Figure S2**. The RHEED patterns of a twin-free film display the diagonal modulation and 3-fold symmetry observed experimentally (**Figure S2a,b**), whereas a film composed of two rotational twins in equal proportion yields 6-fold symmetric patterns with modulated intensity along the diffraction rods (**Figure S2d**).
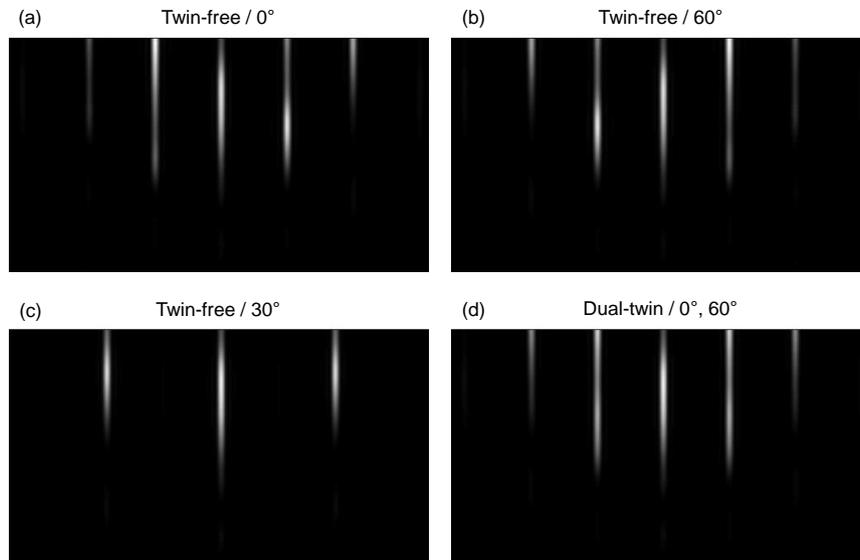

Figure S2. Simulated RHEED patterns of (a-c) a twin-free Bi$_2$Te$_3$ film along different azimuths relative to $[\bar{1}\bar{1}20]$, and (d) a film composed of two twins in equal proportions.

S3. Ab initio calculations

First principle calculations were carried out using density functional theory as implemented in the VASP package.[1] The projected augmented wave method was adopted to treat the core electrons.[2,3] The generalized gradient approximation in the PBE form was used for the exchange-correlation functional.[4] An energy cut-off of 400 eV was chosen together with a $31\times31\times1$ k-point mesh to sample the Brillouin zone. The in-plane lattice constant was set to the one of free BaF_2 (4.384 Å).[5] In order to prevent interaction between neighbor slabs, a 15 Å-thick vacuum zone was considered in the calculation. We also used the Tkatchenko-Scheffler method,[6] which relies on charge density-dependent dispersion coefficient and damping function, to describe the missing dispersion interactions in the whole system during the structure relaxation. We kept the volume of the slab constant, while optimizing the position for each atom along three axes until the forces were smaller than 0.01 eV/Å.

We examined six configurations for Bi_2Te_3 (ABCAB, ACBAC, BACBA, BCABC, CABCA and CBACB) on top of BaF_2, which has a fixed stacking sequence of Ba planes (ABC, by convention, see **Figure S3**). These six configurations correspond to the two possible twins (ABC or ACB order) and to the three possible interfaces with BaF_2 (stacking starting by an A, C or B plane corresponds to Te on top of F, on top of Ba, or in hollow position, respectively). The binding energy of each configuration is reported in **Table S1**. We find that Te in hollow position is the most stable interface, by about 0.1 eV (average BaF_2/Bi_2Te_3 interface energy of +381 meV/cell $\equiv$ +122 mJ/m^2). The energy difference between the BACBA and BCABC twins is 5 meV, in favour of BCABC, as observed experimentally.

The binding energy between Bi_2Te_3 and BaF_2 is quite small (-0.3 ~ -0.4 eV), as well as the charge transfer (~ 0.15 e). All of these results imply that there is no chemical bonding at the interface. The binding energy that only comes from Van der Waals interaction ($E_{B/VdW}$) is slightly higher than the total value E_B; therefore, the binding between Bi_2Te_3 and BaF_2 mainly comes from the Van der Waals force.
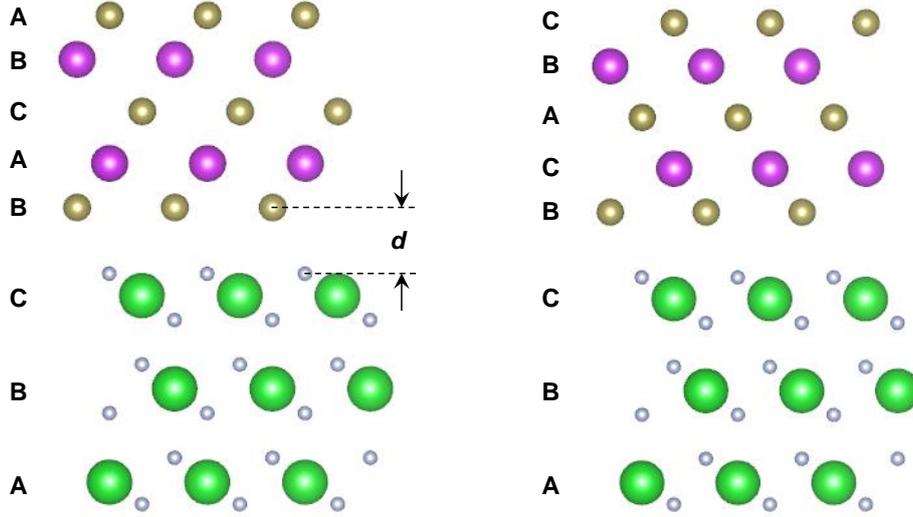
Figure S3. The two most stable configurations for Bi_2Te_3 on top of BaF_2. Brown, purple, white and green colours indicate Te, Bi, F and Ba atoms, respectively. The interlayer spacing is labelled by d.

	d (Å)	ΔE (eV)	E_B (eV)	$E_{B/VdW}$ (eV)
ABCAB	3.114	0.106	-0.278	-0.295
ACBAC	3.110	0.104	-0.280	-0.296
BACBA	2.663	0.005	-0.378	-0.393
BCABC	2.652	0.000	-0.384	-0.392
CABCA	2.883	0.107	-0.277	-0.335
CBACB	2.903	0.107	-0.277	-0.335

$E_B = E_T[Bi_2Te_3/BaF_2] - E_T[BaF_2] - E_T[Bi_2Te_3]$, where E_T is the total energy.

$E_{B/VdW} = E_{VdW}[Bi_2Te_3/BaF_2] - E_{VdW}[BaF_2] - E_{VdW}[Bi_2Te_3]$, where E_{VdW} is the Van der Waals contribution to the total energy.

Table S1. Interlayer spacing and binding energy for different stacking of Bi_2Te_3 on top of BaF_2

References

[1]   G. Kresse, J. Furthmuller, Phys. Rev. B **1996**, 54, 11169.

[2]   P. E. Blochl, Phys. Rev. B **1994**, 50, 17953.

[3]   G. Kresse, D. Joubert, Phys. Rev. B **1999**, 59, 1758.

[4]   J. P. Perdew, K. Burke, M. Ernzerhof, Phys. Rev. Lett. **1996**, 77, 3865.

[5]   S. M. Dorfman, F. Jiang, Z. Mao, A. Kubo, Y. Meng, V. B. Prakapenka, T. S. Duffy, Phys. Rev. B **2010**, 81, 174121.

[6]   A. Tkatchenko, M. Scheffler, Phys. Rev. Lett. **2009**, 102, 073005.